Ultrasonics 95 (2019) 70–78

Contents lists available at ScienceDirect

Ultrasonics

journal homepage: www.elsevier.com/locate/ultras

EMAT design for minimum remnant thickness gauging using high order shear horizontal modes

Aurélien Thon*, Pierre Bélanger

Département de Génie Mécanique, École de Technologie Supérieure, 1100, Rue Notre-Dame Ouest, Montréal, Québec H3C 1K3, Canada

ARTICLE INFO

Keywords:
Ultrasound
Ultrasonic guided waves
Shear horizontal waves
EMAT
Corrosion

ABSTRACT

Detection and sizing of corrosion are critical issues across many industries such as for the oil and gas industry or the petrochemical industry. Inspections may become difficult and time-consuming when the structures under inspection are only partially accessible such as for pipes under insulation or at pipe supports. It has been demonstrated in the literature that the cutoff frequency-thickness product of high order ultrasonic guided wave modes can be used in medium to long-range thickness gauging. As the thickness varies along an inspection line, the thickness variation acts as a low-pass filter for the high order ultrasonic guided wave modes. As the thickness drops below the cutoff frequency-thickness product of a given mode, this mode is filtered out of the propagating wave packet. The effectiveness of this technique depends on the number of excited modes and the width of the ultrasonic beam along the inspection line. Both of these parameters can easily be controlled using electromagnetic acoustic transducers (EMAT) for the excitation. Analytical and multiphysics finite element simulations were performed to optimize an EMAT that can excite enough modes to allow the measurement of the remnant thickness based on the number of modes propagating through a corroded area. The results were validated experimentally, and a thickness resolution of 2 mm was achieved in a 10 mm aluminum plate.

1. Introduction

Corrosion is a major problem across many industries which can lead to catastrophic failures and the ensuing impact on the environment. The gold standard for the quantitative evaluation of the remaining wall thickness remains point-by-point ultrasonic testing [1]. This method is very time-consuming and may become impossible to perform when a structure is only partially accessible such as in the case of pipes under insulation or the evaluation of corrosion at pipe supports. Low-frequency ultrasonic guided waves are nowadays routinely used to screen pipes for corrosion or other defects [2–4]. However, as these techniques essentially use the reflection of non-dispersive fundamental ultrasonic guided wave modes, they can only provide a rough estimate of the remaining wall thickness. Ultrasonic guided waves can be combined with tomographic imaging by using slightly dispersive modes. Ultrasonic guided wave tomography can provide very detailed thickness maps at the expense of using a dense transducer array [5–7]. Moreover, in ultrasonic guided wave tomography, the location of the transducers needs to be controlled with high accuracy so as to obtain accurate thickness maps. Ultrasonic guided wave tomography is also associated with heavy data processing to reconstruct the images.

The alternative that will be developed in this paper is the use of high order shear horizontal guided wave modes (SH waves). High order ultrasonic guided wave modes have the interesting property of only propagating above a certain frequency-thickness product. Previous studies showed that this property could be used to determine the minimum remnant thickness between two points [8–10]. The difficulty identified in the previous studies was the experimental implementation of the technique associated with the choice of the transduction mechanism and the frequency range. Piezoelectric transduction was originally considered in the literature but the coupling of the transducers with the structure under inspection was a major issue. The solution investigated in this paper is the use of periodic permanent magnet (PPM) electromagnetic acoustic transducers (EMAT). PPM EMAT have already been studied extensively to generate the fundamental SH_0 mode at relatively low frequency (< 300 kHz) [11]. However, the method investigated in this paper requires the excitation of a few SH modes.

The purpose of this paper is to evaluate the capabilities of an EMAT to generate a large number of SH modes that will propagate through an area of varying thickness. The SH modes will then be detected and identified on the other side of the varying thickness area, and the minimum remnant thickness will be inferred.

This paper first presents the required theoretical background on SH waves and EMAT optimization to facilitate the use of the cutoff

* Corresponding author.
E-mail address: aurelien.thon@pulets.ca (A. Thon).

https://doi.org/10.1016/j.ultras.2019.03.006
Received 15 November 2018; Received in revised form 12 February 2019; Accepted 4 March 2019
Available online 06 March 2019
0041-624X/

frequency method with high order SH modes. The second section presents a finite element study that was carried out for the optimization of the transducer with the help of Comsol Multiphysics and Pogo [12]. Finally, the simulation results are validated against experiments in the third section. The results are discussed as they are presented.

2. Theoretical background

2.1. Wave propagation

Ultrasonic guided waves are mechanical stress waves that can propagate between the boundaries of waveguides such as plate-like structures. It is possible to separate these mechanical perturbations into two main categories Lamb waves (symmetrical and antisymmetrical) and SH waves. Within each category, there are fundamental modes and high order modes. Fundamental modes (A_0, S_0, and SH_0) can propagate at all frequency-thickness products whereas the high order modes ($A_{1,2,3,...}$, $S_{1,2,3,...}$, $SH_{1,2,3,...}$) can only propagate from a specific frequency-thickness product known as the cutoff frequency-thickness product. Below the cutoff frequency-thickness product, high order modes are considered as vanishing, their energy is reflected or converted into lower order modes [12–14]. When the frequency-thickness product approaches the cutoff frequency-thickness product of high order modes, the phase velocity tends to infinity and the group velocity tends to zero. Fig. 1 presents the phase velocity dispersion curves of Lamb waves and SH waves in an aluminum plate computed using Disperse [15].

Structures damaged by corrosion are generally characterized by a loss of the wall thickness. The consequence for the propagation of a given high order ultrasonic guided wave mode is that a thickness loss may shift the frequency-thickness product below its cutoff frequency-thickness product. Therefore, by identifying the modes that propagate through the thickness loss, it becomes possible to estimate the minimum remnant thickness along the propagation path. The thickness resolution of this method depends on the number of excited modes and

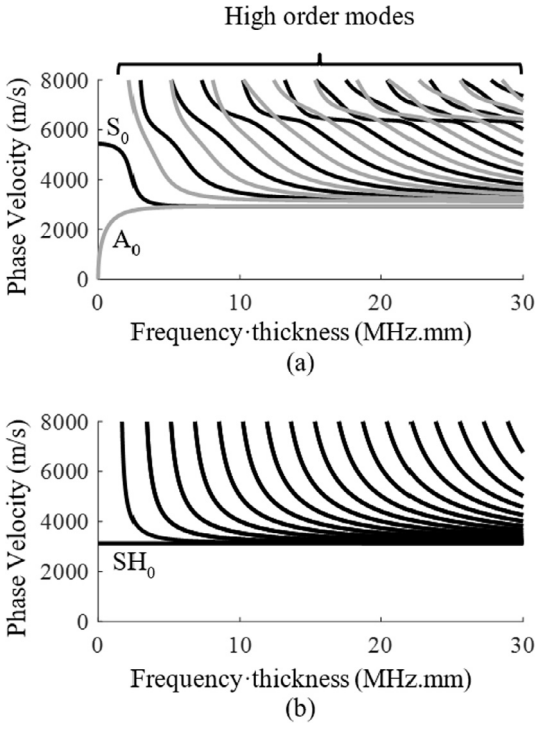

Fig. 1. (a) Lamb waves phase velocity dispersion curves and (b) SH waves phase velocity dispersion curves in an aluminum plate (ρ = 2700 kg/m^3, E = 70 GPa, ν = 0.33).

therefore on the frequency of excitation. A greater number of modes will lead to a better thickness resolution. As shown in Fig. 1(b), all high order SH modes are evenly distributed along the frequency-thickness axis. This interesting property allows the estimation of the minimum remnant thickness on a regular grid. For a given plate thickness h, the cutoff frequency ($f_{cutoff,n}$) of SH mode n can be calculated as follows:

$$f_{cutoff,n} = \frac{nV_s}{2h}, \quad n \in \mathbb{N} \tag{1}$$

where V_s is the bulk shear wave velocity. One other advantage of high order SH modes is that their excitability is constant for a given phase velocity [8]. Morever, SH waves will not convert to Lamb modes when impinging a defect or a feature parallel to the direction of polarization [16]. For those reasons, the rest of the paper will focus solely on high order SH waves.

From Eq. (1) it appears that the highest possible frequency should be used to improve the thickness resolution. However, other aspects must be taken into accounts, such as the uncorroded thickness of the structure and the inspection distance. Indeed, Cheeke [17] showed that the attenuation of a wave can be approximated by:

$$I = I_0 e^{-2\alpha x} \tag{2}$$

where I is the intensity of the wave at a distance x from its source, I_0 is the original intensity and α is a coefficient depending on the material properties and the frequency. High frequencies lead to strong attenuation of the wave and a significant reduction of the inspection distance. Thickness variation due to corrosion also leads to significant scattering therefore further increasing the attenuation. A compromise must therefore be made between the thickness resolution and the inspection distance according to the specifications of the inspection. For the purpose of this study, the inspection distance was arbitrarily set to 0.5 m. This distance is important in the design of the transducers as will be shown in the next subsection.

2.2. Transduction

EMAT refers to a transducer technology using either Lorentz forces, magnetostrictive forces or magnetization forces. They consist, in the simplest state, of two components: an array of magnets and a coil (Fig. 2). The forces f generated by an EMAT can be modelled as follows:

$$\mathrm{f} = \mathrm{f}_L + \mathrm{f}_M \tag{3}$$

$$\mathrm{f}_L = J \times B \tag{4}$$

$$\mathrm{f}_M = \mu_0 \nabla H \hat{\mathrm{A}} \cdot M \tag{5}$$

where f_L is the Lorentz force, f_M is the magnetostrictive force, J is the eddy current induced at the surface of the sample to be inspected, B is the magnetic flux density, H is the magnetic field, M is the magnetization, and μ_0 is the magnetic permeability. In this paper, an aluminum plate will be used for both simulations and experiments and thus only Lorentz forces will be considered since aluminum is not a ferromagnetic material. In a SH wave PPM EMAT, the magnetic field is provided by a set of permanent magnets and the current is induced by a flat and elongated racetrack coil [10,13]. With this concept, the polarity alternation of the magnets allows the generation of SH waves whose wavelength is twice the size of the magnets in the x-direction.

All experiments and simulations were carried out with a 10 mm aluminum plate. The properties of aluminum are considered equal to those used in Fig. 1 (ρ = 2700 kg/m^3, E = 70 GPa, and ν = 0.33) which corresponds to a shear wave velocity of 3130 m/s. An arbitrary thickness loss of 50% was first chosen leading to a 5 mm minimum remnant thickness. The cutoff frequencies of first high order SH modes are summarized in Table 1 for thicknesses of 5 and 10 mm.

At a frequency of 500 kHz, only SH_0 and SH_1 would propagate through a 50% wall thinning area in a 10 mm plate. In this paper, the threshold below which a mode is considered completely reflected or

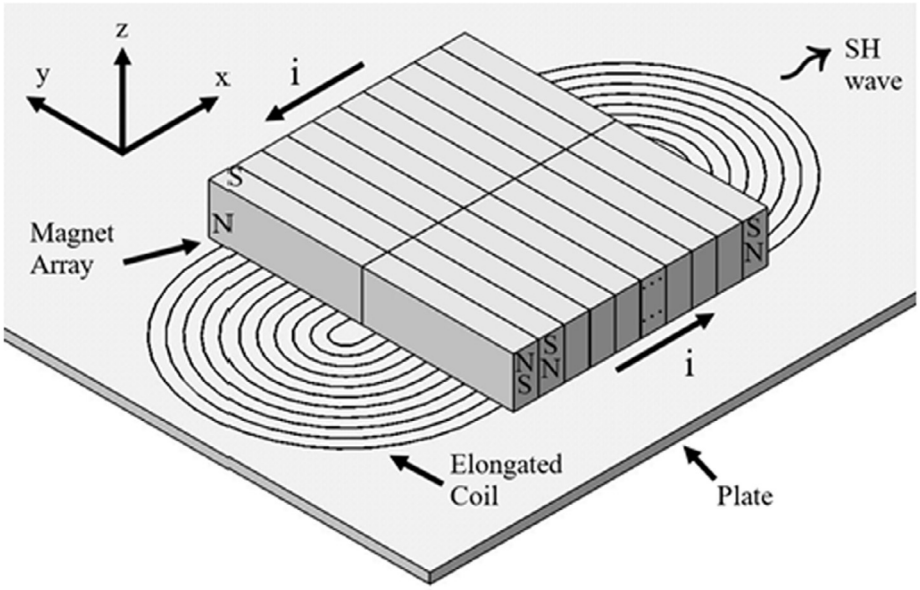

Fig. 2. Schematic of the EMAT used to propagate a directional SH waves using permanent magnets and a racetrack coil.

Table 1
Cutoff frequencies of SH_1 to SH_4 in a 10 mm aluminum plate (ρ = 2700 kg/m^3, E = 70 GPa, ν = 0.33) with a 50% thickness loss (thickness = 5 mm).

Thickness	SH_1	SH_2	SH_3	SH_4
5 mm	313 kHz	626 kHz	939 kHz	1252 kHz
10 mm	156 kHz	313 kHz	469 kHz	626 kHz

converted was arbitrarily set to −20 dB below the mode with the highest amplitude. Considering an excitation signal made from a 3 cycles Hann windowed toneburst centred at 500 kHz the −20 dB frequencies are 225 and 775 kHz (Fig. 3(b)). All modes, except SH_0, SH_1, and SH_2, should therefore be completely reflected or converted to lower order modes.

In a PPM EMAT, the number and size of the magnets determine the wavelength selectivity of the transducer. When considering a PPM EMAT, as in Fig. 2, it is possible to calculate the excited wavenumbers and thus the wavelengths by taking the spatial Fourier transform of the polarization pattern, which is a square function of a period equal to twice the magnet width. Fig. 3(a) shows, as an example, the wavelength selectivity for 20 magnets with dimensions summarized in Table 2.

It is then possible to combine the wavelength selectivity of the transducer with the frequency bandwidth of the input signal to visualize the modes that will be excited as shown in Fig. 3(c).

The combination of these magnets and the input signal transmitted to the coil should, therefore, be able to excite at least the modes SH_0 to SH_3. As SH_4 is on the edge of the frequency bandwidth, its amplitude is expected to be much lower than the other modes. The PPM EMAT described above is therefore compatible with the generation of enough SH modes to detect and size a 50% thickness loss.

Two additional important features to consider in assessing the capabilities of a PPM EMAT to generate SH waves are: (1) the near-field length and (2) the divergence angle of the beam. If the defect is too close to the probe or too small relative to the width of the ultrasonic beam, it may not be detected. These two parameters can be calculated as follows [18]:

$$N = \frac{D^2}{4\lambda} \tag{6}$$

$$\sin\theta = 0.44\frac{\lambda}{D} \tag{7}$$

where N is the length of the near-field, D is the dimension of the transducer in the direction perpendicular to the direction of propagation, λ is the wavelength, and θ is the divergence angle from the centreline to the −6 dB line.

As the received signals comprise up to 4 SH modes, the 2D FFT [19] will be used to separate the modes based on their wavenumber and frequency. To perform the 2D FFT a large number of points must be used in reception. In simulations, reception on a large number of points is not a problem. In experiments, a 2D scanning laser Doppler vibrometer was used to acquire the displacement fields in the direction of polarization of SH waves. The wavenumber-frequency map obtained with the 2D FFT can be converted to the more familiar phased velocity vs frequency graph by using:

$$V_p = \frac{2\pi f}{k} \tag{8}$$

where V_p is the phase velocity, f the frequency, and k the wavenumber.

3. Finite element simulation

By definition, a finite element (FE) simulation corresponds to a discretization of a volume. This discretization implies an error in the calculated values. This error is a decreasing function of the size of the elements. A study by Drozdz et al. [20] showed that a discretization of 10 to 15 elements per wavelength is suitable to simulate the propagation of ultrasonic guided waves using an explicit time stepping simulation scheme. Moreover, the size of the time step must be set such that propagating waves cannot, within one time increment, skip an element [21].

These two criteria have the effect of increasing the computational burden at high frequencies, both regarding the required computing resources as well as the computing time. FE codes using central processing units (CPU) are rapidly limited by the size of the models when the frequency is increasing. Therefore, the use of graphics processing units (GPU) accelerated solvers such as Pogo [12] enables the simulation of very large models with reasonable simulation time and for a relatively low cost of the computing infrastructure when compared with CPU-based FE codes.

Several phenomena are taken into account in the transmission and propagation of ultrasonic waves using EMAT [22] such as (1) the induction of eddy currents due to the coil and to the conductive plate, (2) Lorentz forces due to the presence of variable induced currents and the

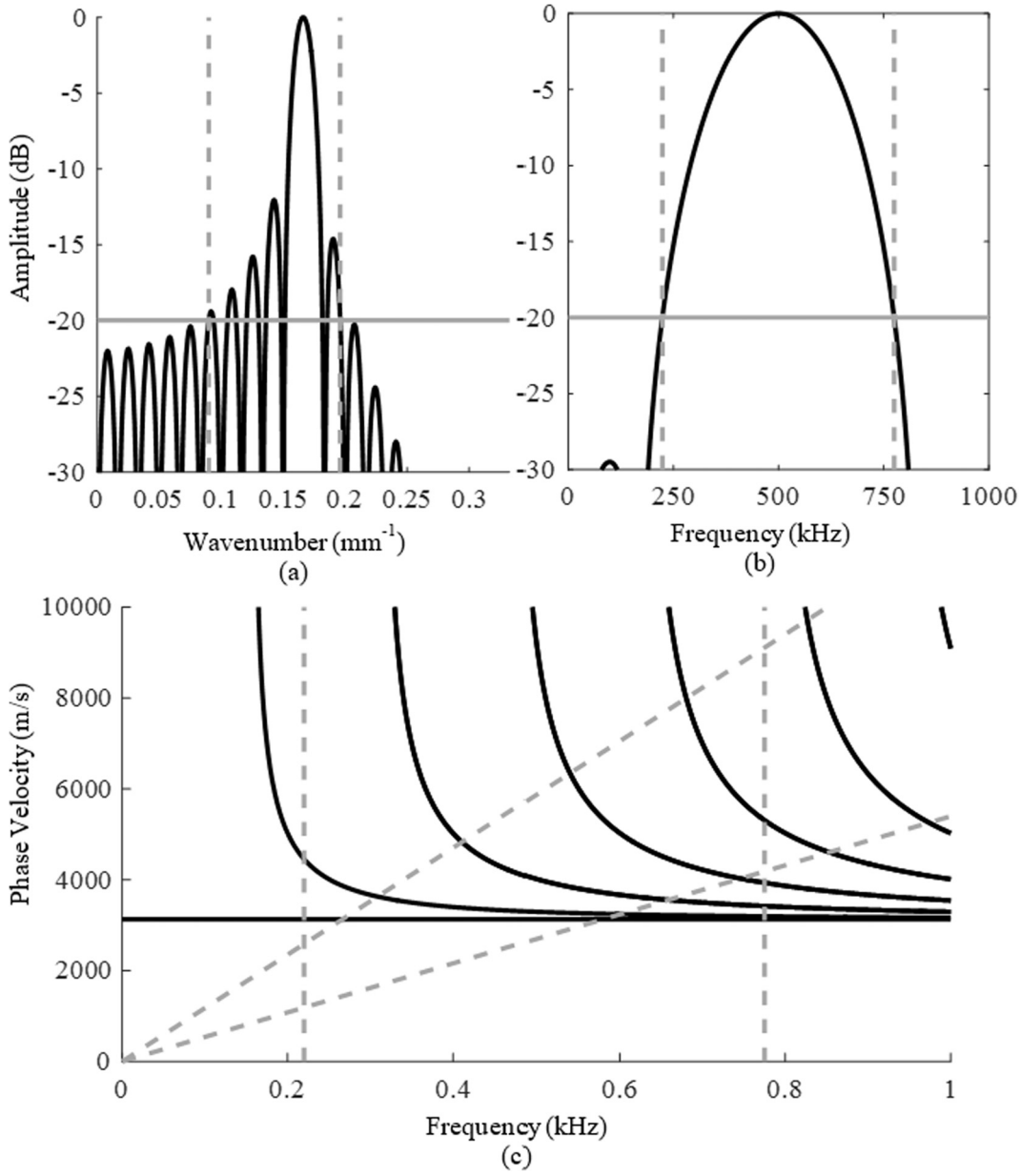

Fig. 3. (a) Amplitude of excitation as a function of the wavenumber with a pitch of 3.175 mm and 20 magnets along the x-axis, (b) Amplitude of excitation as a function of the frequency for a 500 kHz, 3 cycles Hann windowed toneburst, (c) Phase velocity dispersion curves in a 10 mm aluminum plate; with the region of excitation at the intersection of the dash lines.

Table 2
Geometry and magnetization direction of the magnets. The length corresponds to the y dimension, the width to the z, and the thickness to the × (see Fig. 2 for the axis system).

Length (y)	Width (z)	Thickness (x)	Magnetization
25.4 mm	6.4 mm	3.2 mm	Thru Width (z)

constant magnetic field due to magnets or (3) the mechanics of continuous media that characterizes the propagation of ultrasonic guided waves. This type of multiphysics simulations can be handled by certain commercial simulation codes, but they usually do not allow to carry out very heavy simulations such as in the case of ultrasonic wave propagation. The solution used in this paper was to decouple the model. The Lorentz forces were computed in Comsol Multiphysics 5.3a according to the input current, the magnets and the material of the plate. The forces were then imported into a Pogo model to simulate the wave propagation. The propagation of the ultrasonic waves simulated by Pogo was not considered to influence the electromagnetic simulation in Comsol.

A schematic of the transducer and measured points configuration used for both simulations and experiments is shown in Fig. 4. The area of reduced thickness is separated into two sub-regions. Firstly, a region of variable thickness of length L and width W, inside which another region of length L_m and width W_m, where the thickness is constant and corresponds to the minimum remnant thickness. In the case of simulations, L was equal to L_m. In simulations, the transition regions were modeled as half Hann windows. The EMAT was located at a distance from the defect which was at least greater than its near-field length. The measurement points were located downstream of the defect, and the last point was at a distance called the maximum monitoring distance.

The Comsol Multiphysics model comprised three parts: (1) N42 grade magnets, (2) the aluminum plate, and (3) the surrounding air (Fig. 5). The aluminum plate was greatly reduced in size for this

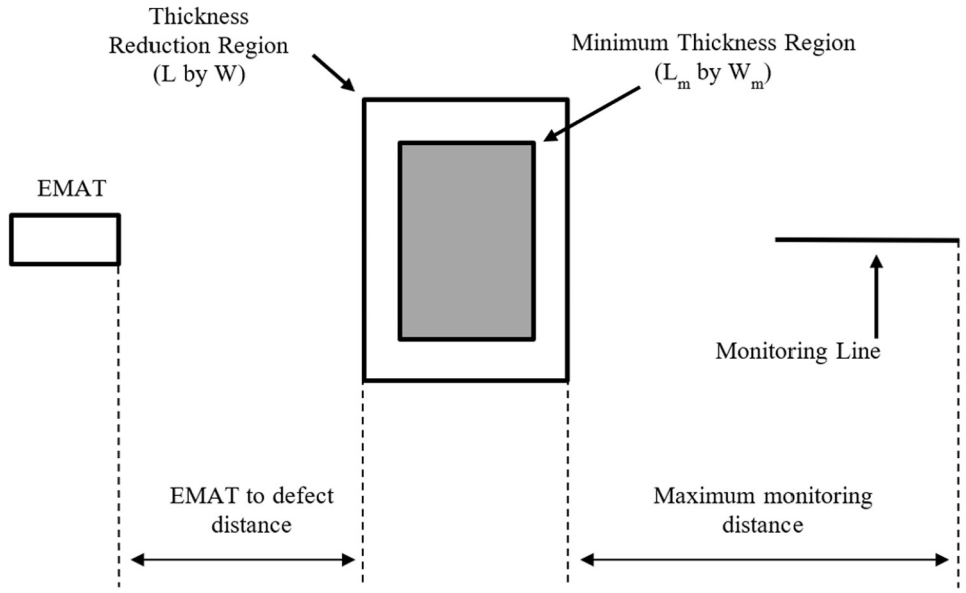

Fig. 4. Schematic of the simulations and the experiments setup. The region of interest where the thickness is varying is located in the far-field of the EMAT and the last monitoring point is located at the maximum monitoring distance.

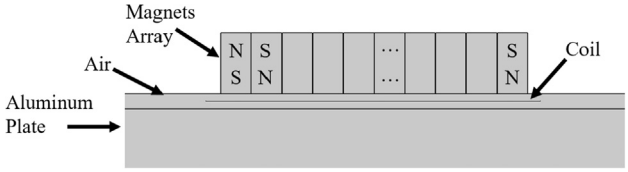

Fig. 5. Schematic of the model used to compute Lorentz Forces using Comsol Multiphysics 5.3a.

modelling step as the Lorentz forces are concentrated under the magnets. The air was located between the magnets and the plate and was surrounding the coil. Its role was mainly to ensure the continuity of the mesh between the magnets and the plate. The input data was therefore the direction of magnetization of the magnets, the current supplied to the coil, and the material of the plate. The magnetic field imposed by the magnets, and the induced eddy currents in the plate were calculated at every node. Lorentz forces can then be obtained using Eq. (4).

Table 3
Near-field and divergence angle values of the ultrasonic beam for different magnet lengths.

Length	N_{an}	N_{fe}	θ_{an}	θ_{fe}
12.7 mm	26 mm	27 mm	6.3°	8.6°
25.4 mm	100 mm	104 mm	3.1°	4.1°
50.8 mm	415 mm	434 mm	1.5°	1.9°

These forces were imported into a plate of uniform thickness in Pogo and the displacement field of the wave propagation was monitored at the plate top surface nodes. The diffraction pattern of the probe is then obtained (Fig. 6). The near-field of the transducer is measured as the distance from the EMAT to the distinct appearance of a conical shape in the displacement field and the angle of divergence equal to half the angle of the aforementioned cone. These finite element values, N_{fe} and θ_{fe}, will then be compared with those obtained using

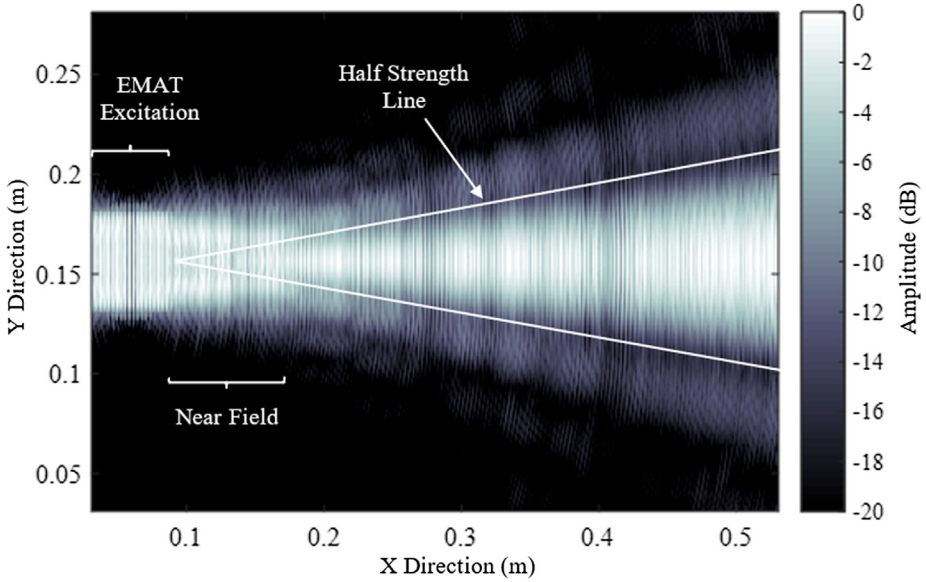

Fig. 6. Diffraction pattern of an EMAT composed of a 2 by 20 array magnets of length 25.4 mm.

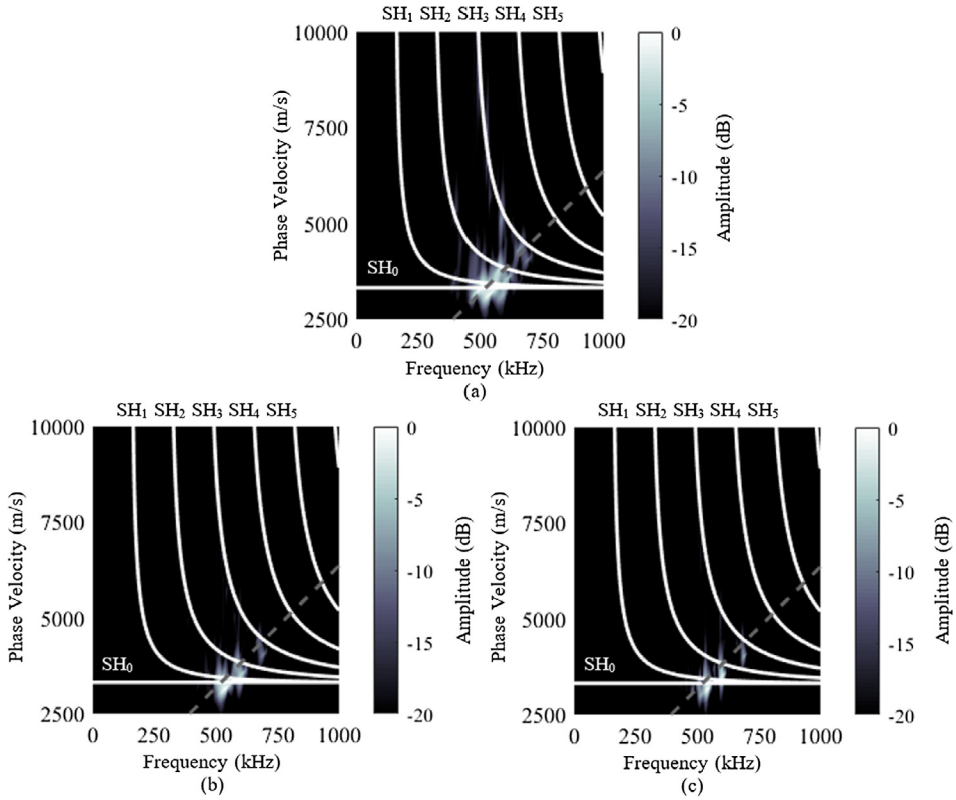

Fig. 7. 2D Fourier transform of signals extracted from simulations shown on a phase velocity frequency map. (a) EMAT composed of 2x10 magnets, (b) 2 × 20 magnets, (c) 2 × 40 magnets. The diagonal grey dashed line corresponds to the wavenumber associated with the pitch of the magnet 1/8″ = 3.175 mm.

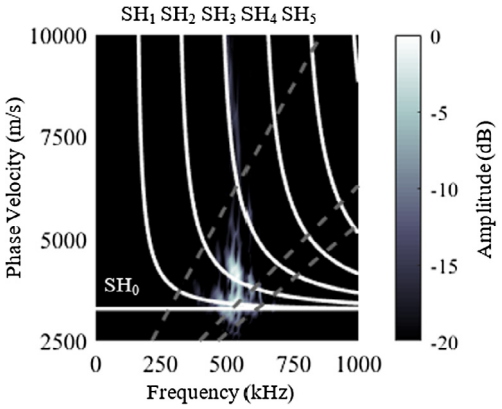

Fig. 8. Phase Velocity diagram computed from simulated data. The EMAT comprised 2 × 20 magnets and the width of the minimum thickness region was 20 mm. Wavenumbers 0.19 mm^{-1} and 0.09 mm^{-1} are represented by the top and bottom diagonal grey dashed lines. The centreline corresponds to the wavenumber associate with the pitch of the magnet 1/8″ = 3.175 mm.

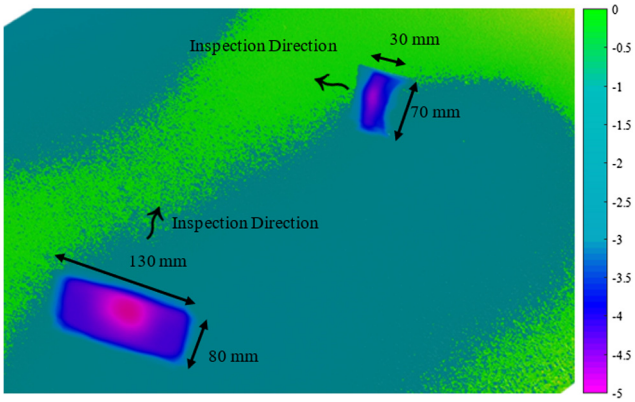

Fig. 9. Scan of the defect on a 10 mm aluminum plate, values correspond to the thickness reduction in mm.

Table 4
Amplitude of the modes affected by a 5 mm thickness loss as a function of the width of the minimum thickness region.

W_m	20 mm	40 mm	60 mm	80 mm
SH_2	−10.8 dB	−10.9 dB	−10.5 dB	−10.2 dB
SH_3	−24 dB	−24.5 dB	−24.9 dB	−24.3 dB

Eqs. (6) and (7), respectively N_{an} and θ_{an}. Simulations were carried out for different values magnets length to select the best compromise. The objective was to obtain a directive probe to be sensitive to small defects but also with a relatively short near-field in order to maximize the inspection length and facilitate manipulation of the probe in the laboratory. In view of the values obtained and summarized in Table 3, the magnets with a length of 25.4 mm were chosen.

The analytical equations were therefore in good agreement with simulations. Using these values, it was then possible to ensure that the position of the defect was in the far-field of the transducer.

The other parameter of interest for the design of the EMAT is the number of magnets. Three different number of magnets were simulated (2 × 10, 2 × 20 and 2 × 40) on a defect-free aluminum plate to verify the number of excited modes. Results are shown in Fig. 7. As predicted in the previous section, an increase in the number of magnets resulted in a reduction of the wavenumber bandwidth. On the phase diagrams, this had the effect of concentrating the energy of the modes around the line corresponding to the central wavenumber of the excitation. This allows an easier separation and identification of the modes when a wall thinning is present in the inspection area. For a 3 cycles Hann

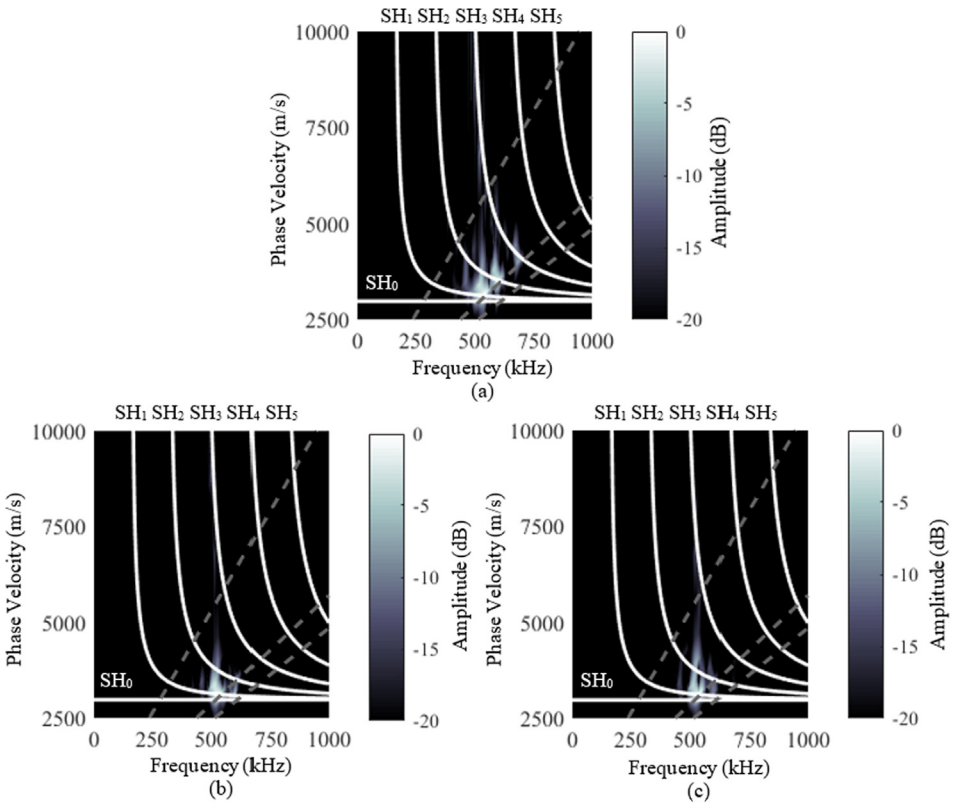

Fig. 10. 2D Fourier transform of signals extracted from simulations shown on a phase velocity and frequency map. (a) No defect, (b) 70 mm by 30 mm defect, (c) 130 mm by 80 mm defect. Wavenumbers $0.19\,mm^{-1}$ and $0.09\,mm^{-1}$ are represented by the top and bottom diagonal grey dashed lines. The centreline corresponds to the wavenumber associate with the pitch of the magnet 1/8″ = 3.175 mm.

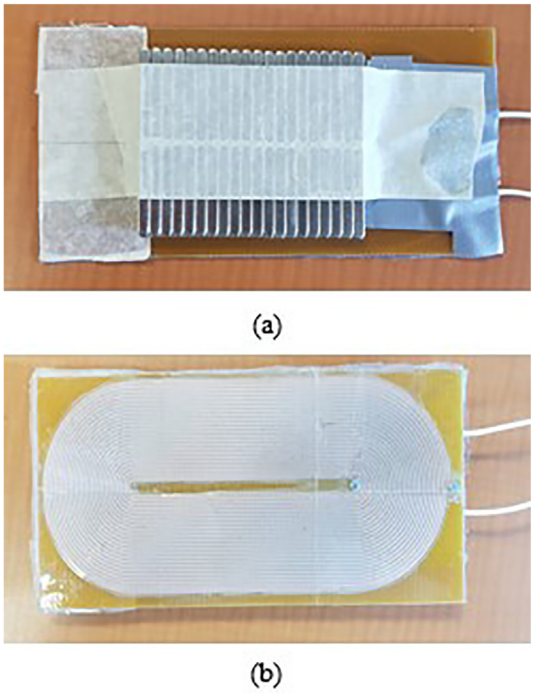

Fig. 11. EMAT with 2 × 20 magnets in top (a) and bottom view (b).

windowed toneburst centred at 500 kHz and the dimensions of the chosen magnets, it is worth noting that the difference between the 20 magnets and 40 magnets case was not significant enough to justify the use of a probe which would be twice as long. For the rest of the paper, a PPM EMAT comprising of 2x20 N42 magnets with the dimensions presented in Table 2 will be used.

Using EMAT design described above, the model was used to verify that the length of the wall thinning region along the propagation direction did not affect the SH mode filtering. For this purpose, a model corresponding to Fig. 4 was produced with a minimum thickness of 5 mm and, by varying the dimension W_m, the amplitudes of the modes affected by the thickness reduction were compared. The results are shown in Fig. 8 and Table 4. It is worth noting that the amplitudes of the modes do not change significantly, in fact the amplitude variation for SH_2 or SH_3 did not exceed 1 dB and showed no trend of divergence.

An aluminum plate was used for the experimental work. Its dimensions were 914 mm by 914 mm and 9.9 mm thick. Two regions were attacked by accelerated corrosion using a saline solution and by applying a potential difference between the plate and an electrode. The plate was then scanned to obtain a thickness map (Fig. 9) using a Metrascan 3D Optical Scanner. The minimum thickness of both corroded areas was 4.9 mm. In the simulations, the dimensions of the plate were reduced to 500 mm in the direction of propagation and 250 mm in the direction perpendicular to the wave propagation. The profiles of the defects were modelled as accurately as possible. To facilitate the comparison with the experimental measurements, a distance of 100 mm between the EMAT and the thickness reduction was fixed. In order to perform the 2D FFT and separate the different modes, a series of 35 measurement points spaced by 1.5 mm was used to detect a maximum wavenumber of $0.67\,mm^{-1}$ and to have a wavenumber detection step of $0.02\,mm^{-1}$. The perimeter of the plate was surrounded by absorbing boundaries designed with the Absorbing Layer with Increasing Damping (ALID) method to reduce the amplitude of the waves reflected by the boundaries and simulate an infinite plate [21–24].

As previously shown in Fig. 10, the excited modes in the defect-free case were SH_0 to SH_3. SH_4 amplitude was too low to be detected. The majority of the energy lied well between the limits provided between 225 and 775 kHz in frequency and between $0.09\,mm^{-1}$ and $0.19\,mm^{-1}$ for wavenumbers. The results in the case of the presence of the thickness reduction were similar for both thickness reductions. SH_3 was filtered out by the thickness reductions, as expected, using the −20 dB threshold. The amplitude of SH_2 was reduced by 10 dB in both cases. The SH_3 mode was excited at a frequency of 710 kHz which, together

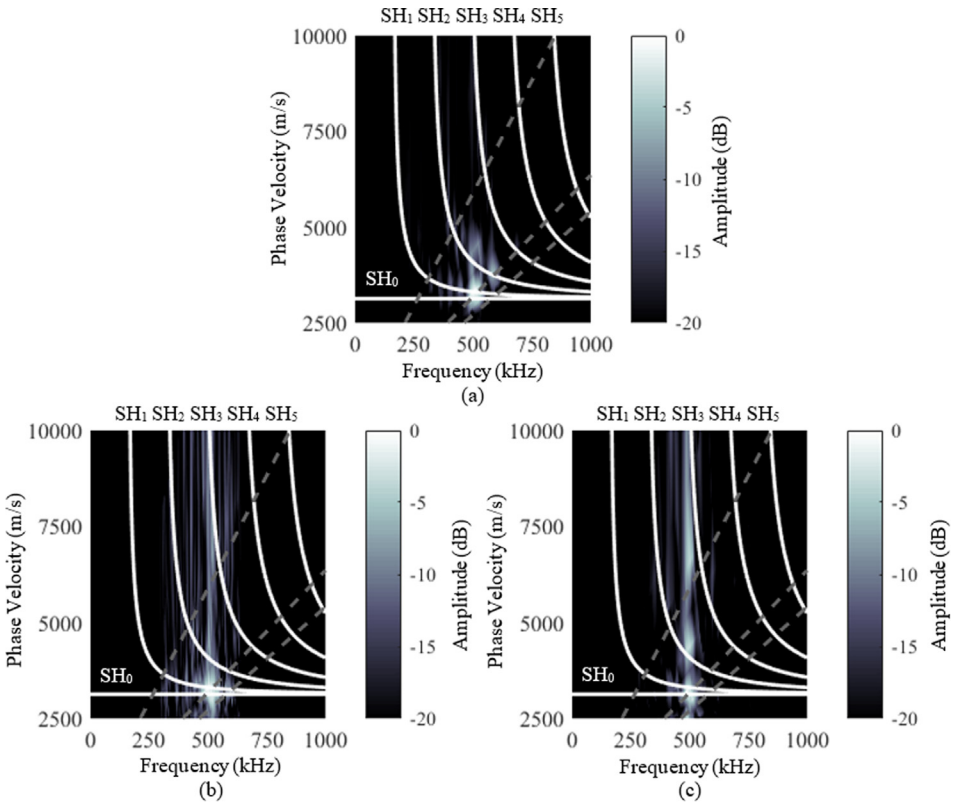

Fig. 12. 2D Fourier transform of signals extracted from experimental measurements shown a phase velocity and frequency map. (a) No defect, (b) 70 mm by 30 mm defect, (c) 130 mm by 80 mm defect. Wavenumbers 0.19 mm^{-1} and 0.09 mm^{-1} are represented by the top and bottom diagonal grey dashed lines. The centreline corresponds to the wavenumber associate with the pitch of the magnet 1/8″ = 3.175 mm.

with the properties of the aluminum used and the fact that it was filtered out, enabled the estimation of the minimum remnant thickness to be less than 6.6 mm (Eq. (1)). SH_2 was excited at a frequency of 610 kHz and was not filtered out which implied that the minimum remnant thickness of the plate was larger than 5.1 mm. Moreover, the sharp decrease of amplitude of SH_2 indicates that the cutoff frequency-thickness product was almost reached which suggests a minimum remnant thickness between the probe and the measurement points close to 5.1 mm. The drop in amplitude of the SH_2 mode was likely due to the group velocity approaching zero and as the time traces were not infinite, SH_2 could not be fully captured.

4. Experimental validation

The prototype EMAT comprised 2x20 neodymium magnets (Table 2) of grade N42. The racetrack coil was manufactured on a printed circuit board (PCB) (Fig. 11). Advantages of such a coil compared to a standard hand-winded coil are a better control of the orientation of the turns, a better repeatability in the manufacturing process of the coil, but also a greater precision in the orientation of the magnets. On this PCB coil, the number of turns was taken so as to cover the entire part of the PCB under the magnets and the spacings on the inner turn made it easier to weld the PCB to the cables without the risk of damaging the other copper tracks. However, the PCB coil manufactured in this project had a substrate thickness of 1.6 mm, therefore, leading to a significant lift-off of the magnets. This thickness could be reduced with other PCB types.

The signal acquisition setup comprised two blocks: (1) the emission and (2) the reception. For the emission, a high-definition 4-channel oscilloscope DSO9024H was used to control an Agilent 33500B signal generator that supplied the desired signal to a Ritec RPR-4000 High Power Pulser Receiver. For the reception, the measurement was performed using a dual-laser Doppler vibrometer system (two Polytec OFV-505, two Polytec controllers OFV-2570) and the DSO9024H oscilloscope. One of the vibrometers measured the normal displacement component at one point and the second was inclined, at a known angle, measuring a superposition of the normal and in-plane displacement components. The inclined laser vibrometer was oriented to measure the displacement component parallel to the surface of the plate in the direction of polarization of SH waves. The in-plane displacement was extracted using trigonometric laws. Reflective tape was used to ensure a good signal-to-noise ratio of both laser heads. The experimental sample was mounted on a motorized XY table to allow the scanning of the region of interest on the plate.

To assess both plate thickness reduction areas effect on the mode cutoff the signal acquisition and processing used was the same as for the simulations. The two areas of reduced thickness had the same minimum remnant thickness but significantly different size. The largest one was 130 mm wide and 80 mm, in the direction of propagation, and the smallest one was 70 mm wide and only 30 mm in the direction of propagation. The EMAT was placed so that the defect was outside the near-field at a minimum distance of 100 mm. The in-plane displacement field was measured on a series of 35 points spaced by 1.5 mm in the direction of propagation starting at a distance of 50 mm from the reduced thickness area.

In the defect-free case (Fig. 12(a)), modes SH_0 to SH_3 were detected with energy evenly distributed among the excited modes. Energy lied well between the limits provided between 225 and 775 kHz in frequency and between 0.09 mm^{-1} and 0.19 mm^{-1} for wavenumbers. In both cases, with the presence of a thickness reduction (Fig. 12(b and c)), the complete cutoffs of SH_2 and SH_3 modes were observed. With the same reasoning as for the simulations, it can be deduced that the absence of the SH_2 mode implied a minimum remnant thickness of less than 5.1 mm. The propagation of the SH_1 mode through the defect leads to a minimum remnant thickness of more than 3 mm. In simulations, SH2 was not completely filtered out but a significant drop in its amplitude was observed. This is likely due to the slightly different material properties in the simulation and the experiments leading to a small shift in the dispersion curves. Indeed, the shear wave speed is 3130 m/s for simulations compared to 3160 m/s in the aluminum plate used for the

experiments. The size of the thickness reduction did not appear to have a significant effect on the results when the minimum remnant thickness remains the same (see Fig. 12(b and c)) as was observed in the simulations. This result is very encouraging as the method was sensitive to the minimum remnant thickness even for a relatively small thickness reduction (70 mm by 30 mm). Moreover, for the small reduced thickness patch, the minimum remnant thickness was concentrated on an area of only 35 mm wide and 12 mm in the direction of propagation.

5. Conclusions

The ability of an EMAT to generate high order SH modes compatible with the structural filtering process was theoretically demonstrated using FE simulations and confirmed experimentally. The simulations were used to design a prototype EMAT for the experimental implementation of the method. In simulations, the minimum remnant thickness between the probe and the measurement points was estimated to be between 5.1 mm and 6.6 mm. However, as the amplitude SH_2 was significantly reduced, suggesting that the mode got very close to its cutoff, a minimum remnant thickness close to 5.1 mm was estimated. In experiments, two thickness reduction areas were tested: a relatively large patch 130 mm wide by 80 mm in the direction of propagation and a smaller patch 70 mm wide by 30 mm in the direction propagation. Both reduced thickness patches had the same minimum remnant thickness of 4.9 mm. The interpretation of the experimental dispersion curves showed a minimum remnant thickness for both patches in the range between 3 mm and 5.1 mm. The experimental thickness resolution, in this case, is relatively low but the correct range of minimum remnant thickness was identified.

Acknowledgments

We would like to thank Nvidia for providing us with a Nvidia Quadro P6000 graphics card for our GPU simulations. The authors would also like to thank the Natural Sciences and Engineering Research Council of Canada and Olympus NDT Canada for funding this project.

References

[1] J. Krautkrämer, H. Krautkrämer, Ultrasonic Testing of Materials, Springer, Berlin Heidelberg, Berlin, Heidelberg, 1990.
[2] D.N. Alleyne, M.J.S. Lowe, P. Cawley, The reflection of guided waves from circumferential notches in pipes, J. Appl. Mech. 65 (3) (1998) 635–641.
[3] D.N. Alleyne, B. Pavlakovic, M.J.S. Lowe, P. Cawley, Rapid, long range inspection of chemical plant pipework using guided waves, AIP Conf. Proc. 557 (1) (2001) 180–187.
[4] P.J. Mudge, Field application of the Teletest; Long-range ultrasonic testing technique, Insight 43 (2) (2001) 74–77.
[5] P. Belanger, P. Cawley, F. Simonetti, Guided wave diffraction tomography within the born approximation, IEEE Trans. Ultrason. Ferroelectr. Freq. Control 57 (6) (2010) 1405–1418.
[6] P. Huthwaite, F. Simonetti, High-resolution guided wave tomography, Wave Motion 50 (5) (2013) 979–993.
[7] J. Rao, M. Ratassepp, Z. Fan, Guided Wave Tomography Based on Full Waveform Inversion, IEEE Trans. Ultrason. Ferroelectr. Freq. Control 63 (5) (2016) 737–745.
[8] P. Belanger, High order shear horizontal modes for minimum remnant thickness, Ultrasonics 54 (4) (2014) 1078–1087.
[9] J.L. Rose, J. Barshinger, Using ultrasonic guided wave mode cutoff for corrosion detection and classification, 1998 Proceedings of the IEEE Ultrasonics Symposium (Cat. No. 98CH36102), 1998, pp. 851–854.
[10] M. Hirao, H. Ogi, An SH-wave EMAT technique for gas pipeline inspection, NDT E Int. 32 (3) (1999) 127–132.
[11] M. Hirao, H. Ogi, EMATs for Science and Industry: Noncontacting Ultrasonic Measurements, Springer, US, 2003.
[12] P. Huthwaite, Accelerated finite element elastodynamic simulations using the GPU, J. Comput. Phys. 257 (2014) 687–707.
[13] N. Nakamura, H. Ogi, M. Hirao, Mode conversion and total reflection of torsional waves for pipe inspection, Jpn. J. Appl. Phys. 52 (7S) (2013).
[14] N. Nurmalia, H. Nakamura, M. Hirao Ogi, K. Nakahata, Mode conversion behavior of SH guided wave in a tapered plate, NDT E Int. 45 (1) (2012) 156–161.
[15] B. Pavlakovic, M. Lowe, D. Alleyne, P. Cawley, Disperse: a general purpose program for creating dispersion curves, Review of Progress in Quantitative Nondestructive Evaluation, Springer, Boston, MA, 1997, pp. 185–192.
[16] P.A. Petcher, S.E. Burrows, S. Dixon, Shear horizontal (SH) ultrasound wave propagation around smooth corners, Ultrasonics 54 (4) (2014) 997–1004.
[17] J.D.N. Cheeke, Fundamentals and Applications of Ultrasonic Waves, second ed., CRC Press, 2016.
[18] Olympus, Introduction to Phased Array Ultrasonic Technology Applications, 2004.
[19] D. Alleyne, P. Cawley, A two-dimensional Fourier transform method for the measurement of propagating multimode signals, J. Acoust. Soc. Am. 89 (3) (1991) 1159–1168.
[20] M. Drozdz, L. Moreau, M. Castaings, M.J.S. Lowe, P. Cawley, Efficient numerical modelling of absorbing regions for boundaries of guided waves problems, AIP Conf. Proc. 820 (1) (2006) 126–133.
[21] R.D. Cook, D.S. Malkus, M.E. Plesha, R.J. Witt, Concepts and Applications of Finite Element Analysis, John Wiley & Sons Inc, USA, 2007.
[22] R. Ribichini, Modelling of electromagnetic acoustic transducers, p. 154.
[23] M.B. Drozdz, Efficient finite element modelling of ultrasound waves in elastic media, Ph.D Imperial College, London, 2008.
[24] P. Rajagopal, M. Drozdz, E.A. Skelton, M.J.S. Lowe, R.V. Craster, On the use of absorbing layers to simulate the propagation of elastic waves in unbounded isotropic media using commercially available Finite Element packages, NDT E Int. 51 (2012) 30–40.